ACADEMIC PRESS

Available online at www.sciencedirect.com

SCIENCE DIRECT®

Journal of Sound and Vibration 268 (2003) 249–267

JOURNAL OF SOUND AND VIBRATION

www.elsevier.com/locate/jsvi

Conditions for the excitation of interface waves in a thin unconsolidated sediment layer

Michael A Ainslie*

TNO Physics and Electronics Laboratory, Underwater Acoustics Group, Oude Waalsdorperweg 63, 2509 JG The Hague, Netherlands

Received 8 July 2002; accepted 11 November 2002

Abstract

The reflection of a plane acoustic wave from the seabed is considered. Conditions for the generation of an interface wave in a thin unconsolidated sediment layer overlying a solid substrate are examined, with particular attention to a resonance excited at low frequency and near grazing incidence. Assuming that the sediment layer can be treated as a fluid, the main requirement is for the sediment–substrate impedance ratio (evaluated at grazing incidence) to be less than -1, and very high reflection loss is shown to arise when this condition is only just met. The bottom reflection loss is evaluated at resonance for realistic combinations of seabed parameters, and lower limits are placed on the substrate compressional and shear speeds required for the high losses to occur. Finally, the influence of a small non-zero sediment rigidity is considered.

1. Introduction

A plane acoustic wave in water incident on the seabed, comprising a thin unconsolidated sediment layer overlying a uniform solid (rock) substrate, is considered. It is well known that, given the right conditions, it is possible to excite high-amplitude evanescent waves in a fluid sediment, resulting in high reflection losses when the acoustic wavelength is comparable with the sediment thickness. Hawker [1,2] shows that a Scholte wave can be excited at the lower boundary, the conditions for which are investigated by Hovem and Kristensen [3], who demonstrate the existence of a second type of interface wave excited at a lower frequency and near grazing incidence. Ainslie [4] considers the same seabed model as Hovem and Kristensen and investigates the variation of acoustic intensity with depth and angle, in the sediment layer, for both types of

*Tel.: +31-70-3740491; fax: +31-70-3740654.
E-mail address: ainslie@fel.tno.nl (M.A. Ainslie).

0022-460X/03/$ - see front matter
doi:10.1016/S0022-460X(03)00203-7

waves. Here, attention is focused on the low-frequency feature which is associated with a resonant evanescent wave. In Section 2 a formula is derived for the resonance frequency and some illustrative reflection loss calculations are presented. The conditions required for the existence of both features are described in Section 3, illustrated by examples from the literature. Section 4 calculates the reflection loss vs. angle at resonance and investigates how this function varies with sediment type for three different substrates based on data from Christensen and Salisbury [5]. It is shown that exceptionally high losses are incurred, over a broad range of frequencies, when the combination of sediment and substrate parameters is such that the Section 3 criterion is only just met. The sediment parameters are chosen to represent different grades of silt, sand and gravel, using correlations between sound speed, density, attenuation and grain size published by Hamilton and Bachman [6,7]. Important additional effects due to rigidity of the sediment layer [8] are acknowledged and these are discussed briefly in Section 5, but mostly ignored for the sake of simplicity.

Following Cagniard [9], the term 'Scholte' wave is used to mean the interface wave that propagates along the boundary between a fluid and a solid, described in his Appendix II, consistent with the definition of Morfey [10]. In some earlier work, this type of wave is referred to as a 'Stoneley' wave [1–4,11]. 'Scholte' is used here to avoid confusion with the alternative use of 'Stoneley' for the interface wave at the boundary between two solids, travelling more slowly than the shear speed in either medium [10,12].

2. Reflection coefficient

Consider the seabed of Fig. 1, comprising a fluid sediment layer of sound speed c_2 and thickness h, overlying a solid substrate of compressional speed c_3^p and shear speed c_3^s. (The figures use the shorthand c_p and c_s for these last two parameters.) The sediment is assumed to be sufficiently thin to neglect refraction within the layer. It is further assumed that c_2, c_3^p and c_3^s are all larger than c_1,

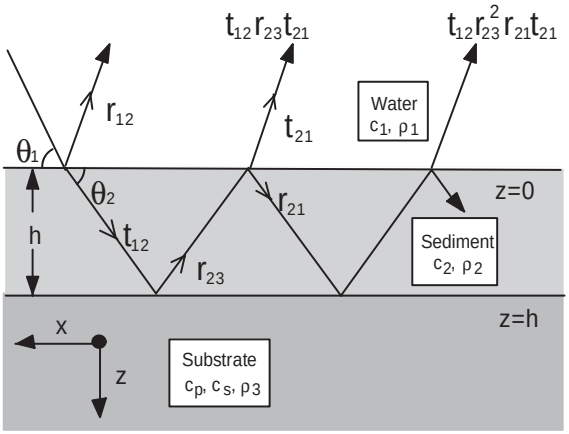

Fig. 1. Illustration of the seabed model and ray path geometry. The boxes indicate the notation used in each of the three layers for wave speed c_i and density ρ_i.

the sound speed in water, so that the corresponding critical angles α_i^μ exist and are given by

$$\cos\alpha_i^\mu = c_1/c_i^\mu, \tag{1}$$

where c_i^μ is any one of c_2, c_3^p, c_3^s. (In the case of a fluid sediment, the superscript is superfluous for layer 2.) For an incident plane wave in the water of angular frequency ω and grazing angle θ_1, the corresponding vertical wave numbers are

$$\gamma_i^\mu = (\omega/c_i^\mu)\sin\theta_i^\mu, \tag{2}$$

where the angles θ_i^μ are related by Snell's law, such that $c_i^\mu \sec\theta_i^\mu$ is a constant. Finally, it is assumed that energy dissipation occurs either in the sediment or substrate, but not necessarily in both.

The reflection coefficient can be written in the form [13]

$$r = (r_{12} + r_{23})/(1 + r_{12}r_{23}), \tag{3}$$

where r_{12} and r_{23} are the water–sediment and sediment–substrate reflection coefficients

$$r_{12} = (\zeta_{12} - 1)/(\zeta_{12} + 1), \tag{4}$$

$$r_{23} = [(\zeta_{23} - 1)/(\zeta_{23} + 1)]\exp(2i\gamma_2 h). \tag{5}$$

Notice the two-way phase term in r_{23}, essential to account correctly for interference effects. If the wave is an evanescent one, then γ_2 is imaginary and in that case the exponential term represents an amplitude ratio. The impedance ratios ζ_{ij} are

$$\zeta_{12} = \frac{\rho_2\gamma_1}{\rho_1\gamma_2} \tag{6}$$

and

$$\zeta_{23} = \frac{\rho_3\gamma_2}{\rho_2}\left(\frac{\cos^2 2\theta_3^s}{\gamma_3^p} + \frac{\sin^2 2\theta_3^s}{\gamma_3^s}\right). \tag{7}$$

Fig. 2 shows the reflection loss ($-20\log_{10}|r|$) plotted vs. dimensionless frequency K (defined as $\omega h/c_2$) and angle θ_1 for the parameters of Table 1, corresponding to a sand sediment overlying a basalt substrate (see Appendix A). The features marked "S" and "E" are due to the excitation, respectively, of a Scholte wave at the sand–basalt boundary, and a resonant evanescent wave in the sand layer. The Scholte wave is associated with a large tangential component of intensity at the bottom of the sediment [4] and travels at a speed (Eq. (2.98) of Ref. [14]) of 1653 m/s, in agreement with the observed grazing angle of 22°. The evanescent resonance is excited near grazing incidence and for a single sharply defined frequency. In both cases the high losses can be explained by cancellation between r_{12} and r_{23} in the numerator of Eq. (3). For the evanescent resonance this happens at grazing incidence such that $r_{12} \approx -1$ and $r_{23} \approx +1$. The corresponding frequency then follows by taking the logarithm of Eq. (5):

$$K_E = \frac{\cot\alpha_2}{2}\ln\frac{(\zeta_0 - 1)}{(\zeta_0 + 1)}, \tag{8}$$

where ζ_0 is the impedance ratio ζ_{23} evaluated at $\theta_1 = 0$. For the parameters of Table 1, Eq. (8) predicts a resonance at a dimensionless frequency K_E of 1.1, consistent with Fig. 2. For a sediment thickness of 1 m, this would correspond to a resonance frequency of 320 Hz.

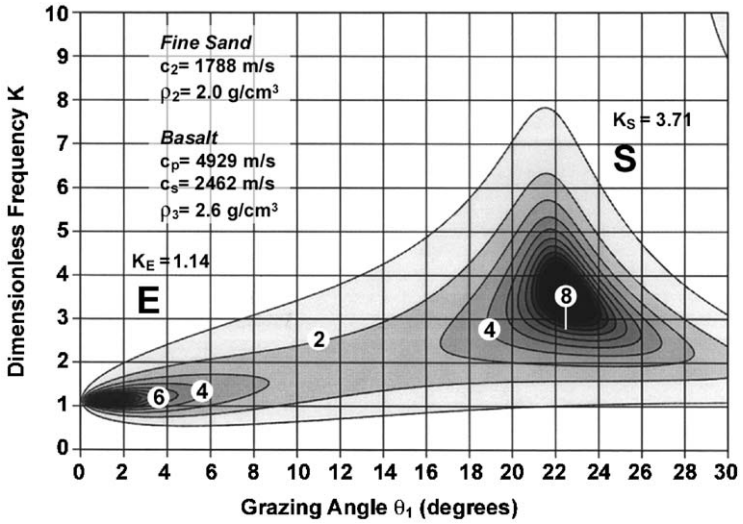

Fig. 2. Plane wave reflection loss vs. grazing angle θ_1 and dimensionless frequency K for a fluid sand sediment overlying a basalt substrate (see Table 1). Contour levels are 1–10 dB in 1 dB steps.

Table 1
Seabed model for Fig. 2

Layer i	Density ρ_i (g/cm^3)	Compressional speed c_i^p (m/s)	Compressional attenuation β_i^p (dB/λ)	Shear speed c_i^s (m/s)	Shear attenuation β_i^s (dB/λ)
1 (water)	1.025	1538	0.0	—	—
2 (sand)	2.035	1788	0.868	—	—
3 (basalt)	2.600	4929	0.100	2462	0.2

3. Conditions for high loss

3.1. General criterion

It follows by inspection of Eq. (8) that a real solution is possible if and only if

$$\zeta_0 < -1 \tag{9}$$

and this same inequality ensures that the requirement for a Scholte wave ($\zeta_{23} + 1 = 0$) can also be satisfied. This is because for the assumed conditions ($c_3^p > c_3^s > c_1$), ζ_{23} increases from ζ_0 at $\theta_1 = 0$ to a non-negative value at the critical angle. Thus, inequality (9) is a necessary and sufficient condition for the existence of both S and E features. (The frequency limits between which they occur are derived in Section 3.2 below.)

From Eq. (7) it is found that

$$\zeta_0 = \frac{\rho_3 \sin\alpha_2}{\rho_2}\left[\operatorname{cosec}\alpha_3^p - 4\tan^2\alpha_3^s \sec^2\alpha_3^s(\operatorname{cosec}\alpha_3^s - \operatorname{cosec}\alpha_3^p)\right] \tag{10}$$

and Eq. (9) can therefore be expressed as a lower limit either on α_2

$$\rho_2 \operatorname{cosec}\alpha_2 < \rho_3[4\tan^2\alpha_3^s \sec^2\alpha_3^s(\operatorname{cosec}\alpha_3^s - \operatorname{cosec}\alpha_3^p) - \operatorname{cosec}\alpha_3^p] \tag{11}$$

or on α_3^p

$$\operatorname{cosec}\alpha_3^p < \frac{4\tan\alpha_3^s \sec^3\alpha_3^s - (\rho_2/\rho_3)\operatorname{cosec}\alpha_2}{4\tan^2\alpha_3^s \sec^2\alpha_3^s + 1}. \tag{12}$$

Figs. 3 and 4 illustrate these two inequalities in graphical form and can be used to predict whether a particular combination of parameters will result in high losses for a fluid sediment. Fig. 3 shows threshold values of $(\rho_2/\rho_3)\operatorname{cosec}\alpha_2$ as a function of $\cos\alpha_3^s$ and $\sqrt{2}\cos\alpha_3^p$. For a given combination of c_3^p and c_3^s, one can read off a value for the threshold, equal to 2.6 for the Table 1 parameters. High losses arise unless this threshold is exceeded. The actual value of $(\rho_2/\rho_3)\operatorname{cosec}\alpha_2$ for the sand–basalt seabed parameters is 1.5, less than the threshold and therefore consistent with observed high losses. The white region of Fig. 3 below indicates combinations of α_3^p and α_3^s for which high losses cannot arise for the mechanisms considered here. Increasing darkness levels in Fig. 3 indicate an increasing threshold and therefore, for a sediment material selected at random, increasing likelihood of high losses. The shaded region above the diagonal is forbidden on physical grounds, corresponding to combinations leading to negative values of the Poisson ratio. Below the diagonal, there is a more lightly shaded region (in the shape of a delta wing) indicating the expected range of material properties for rocks, based on Fig. 11 of Ludwig et al. [15].

For the condition on α_3^p, it is convenient to rewrite inequality (12) as an upper limit on $\cos^2\alpha_3^p$ in the form

$$\frac{\cos^2\alpha_3^p}{\cos^2\alpha_3^s} < \frac{\left[4\tan\alpha_3^s \sec^3\alpha_3^s - (\rho_2/\rho_3)\operatorname{cosec}\alpha_2\right]^2 - (4\tan^2\alpha_3^s \sec^2\alpha_3^s + 1)^2}{[4\tan\alpha_3^s \sec^2\alpha_3^s - (\rho_2/\rho_3)\cos\alpha_3^s \operatorname{cosec}\alpha_2]^2}. \tag{13}$$

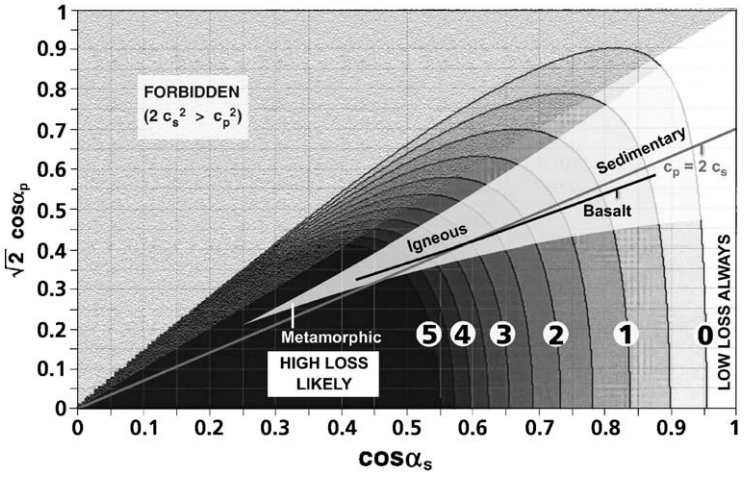

Fig. 3. Contours of $(\rho_2/\rho_3)\operatorname{cosec}\alpha_2$ threshold for use with inequality (11). Contour levels are 0–5 in steps of 0.5. The white region on the right marked "LOW LOSS ALWAYS" indicates conditions for which high losses cannot arise from the generation of interface waves, irrespective of sediment properties. The black region indicates that high losses are likely but not inevitable.

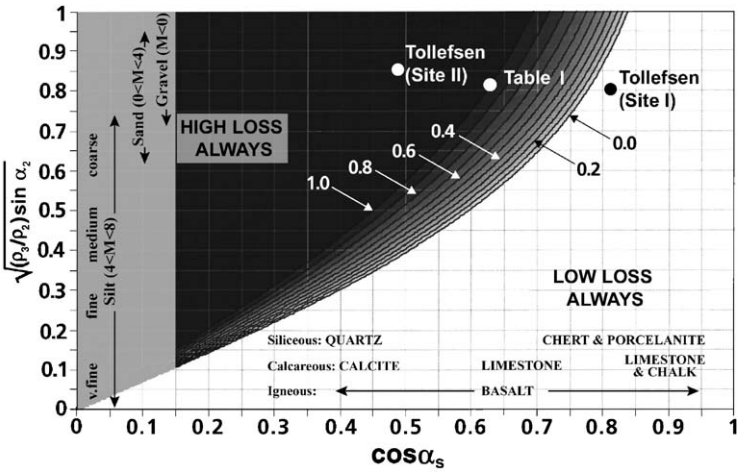

Fig. 4. Contours of $2(c_3^s/c_3^p)^2$ threshold for use with inequality (13). Contour levels are 0–1 in steps of 0.1. The white region on the right marked "LOW LOSS ALWAYS" indicates conditions for which high losses cannot arise from the generation of interface waves. Conversely, in the black region high losses are inevitable, irrespective of the substrate sound speed c_3^p.

Fig. 4 shows threshold values of $2\cos^2\alpha_3^p/\cos^2\alpha_3^s$ plotted as a function of $\cos\alpha_3^s$ and $\sqrt{(\rho_3/\rho_2)}\sin\alpha_2$. It is similar to Hovem and Kristensen's [3] Fig. 7 except that here any combination of ρ_3, ρ_2 and c_3^p is allowed (their Fig. 7 is restricted to $c_3^p/c_3^s = 2$ and $\rho_3/\rho_2 = 5/4$), with the transition region between high and low losses shown explicitly. Fig. 4 annotation is based on Udden [16] for sediments (y-axis) and Hamilton [17] for rocks (x-axis).

Also apparent from Fig. 3 are *absolute* upper limits on $\cos\alpha_3^p$ and $\cos\alpha_3^s$ of $(\sqrt{5}-1)/2 = 0.618$ and $\left(13+\sqrt{297}\right)/8\sqrt{2} = 0.955$, respectively [4], for which high losses are possible due to interface waves. A necessary condition is therefore that $\alpha_3^p > 51.8^\circ$ and $\alpha_3^s > 17.2^\circ$ must both be satisfied, implying, for a nominal sound speed in water of 1500 m/s, that $c_3^p > 2430$ m/s and $c_3^s > 1570$ m/s. In practice, though, the substrate wave speeds need to be considerably larger than these theoretical limits suggest. To derive more realistic (though approximate) limits, note first that inequality (11) is a function of sediment properties only on the left-hand side (LHS) and of substrate properties on the right (RHS). Furthermore, because of correlations between the various material properties [6,17,18], one can write the RHS and LHS as a function of the critical angle α_3^s and sediment density ρ_2, respectively:

$$RHS(\alpha_3^s) = \rho_3(\alpha_3^s)\left\{4\tan\alpha_3^s\sec^3\alpha_3^s - \frac{1+4\tan^2\alpha_3^s\sec^2\alpha_3^s}{\left[1-(c_3^s/c_3^p)^2\cos^2\alpha_3^s\right]^{1/2}}\right\} \tag{14}$$

and

$$LHS(\rho_2) = \rho_2\left\{1-\left[\frac{c_1}{c_2(\rho_2)}\right]^2\right\}^{-1/2}. \tag{15}$$

For the functions $c_2(\rho_2)$ and $\rho_3(\alpha_3^s)$, respectively, the sound speed vs. density equation is used for continental terrace sediments from Ref. [6]:

$$c_2(\rho_2) = 2330.4 - 1257.0\rho_2 + 487.7\rho_2^2 \tag{16}$$

and curve G from Hamilton's [17] Fig. 7 (due to Gardner et al. [19])

$$\rho_3(\alpha_3^s) = 0.23\left[\frac{(c_3^p/c_3^s)c_1}{0.3048\cos\alpha_3^s}\right]^{1/4}, \tag{17}$$

where all sound speeds are in units of m/s and densities in g/cm^3. With these substitutions, Eq. (15) for the LHS has a minimum of 3.4 g/cm^3. High losses are therefore unlikely, unless the RHS exceeds this value. Assuming a ratio $c_3^p/c_3^s \approx 2$ [18], the condition becomes $\alpha_3^s > 42^\circ (c_3^s > 2020\,\text{m/s})$ and hence $\alpha_3^p > 68^\circ (c_3^p > 4040\,\text{m/s})$. These conditions do not provide rigorous absolute limits, but reasonable lower bounds on these parameters. The possibility of intermediate shear speeds (1570–2020 m/s) giving rise to high interface wave losses is not ruled out, but such occurrences are expected to be rare.

3.2. Frequency limits

High losses due to interface waves are generated in a specific range of frequencies, the lower limit of which is the evanescent resonance frequency K_E. The upper limit is less well defined, but can be estimated by considering the behaviour of $|r_{23}|$ (evaluated at the Scholte angle) with frequency. At low frequency, this quantity, denoted $r_\sigma(K)$, becomes very large due to the $\zeta_{23} + 1$ denominator, and at high frequency it tends to zero due to the $\exp[-2h\,\text{Im}(\gamma_2)]$ factor. Therefore, there must be a maximum frequency for which $|r_\sigma(K)|$ can be equal to unity, thus allowing the necessary cancellation between r_{12} and r_{23}. From Eq. (5) one sees that the critical frequency (K_S) above which this cancellation becomes impossible is given by

$$2|\sin\theta_2|K_S = \ln\left|\frac{1-\zeta_\sigma}{1+\zeta_\sigma}\right|, \tag{18}$$

where ζ_σ is the value of ζ_{23} evaluated at the Scholte angle. The real part of ζ_σ is equal to -1; so K_S is determined by $\text{Im}(\zeta_\sigma)$, which depends in turn on the imaginary parts of c_2, c_3^p and c_3^s. Assuming that the interface wave attenuation is dominated by absorption in the sediment (rather than in the substrate), it follows that

$$\zeta_\sigma = -1 + \frac{i\delta_2/2\pi}{\left|(c_2/\sigma)^2 - 1\right|}, \tag{19}$$

where δ_2 is the sediment absorption coefficient (in nepers per wave length) and σ is the Scholte wave speed, so that Eq. (18) becomes

$$2|\sin\theta_2|K_S = \ln\frac{4\pi\left|(c_2/\sigma)^2 - 1\right|}{\delta_2}. \tag{20}$$

As defined above, the critical frequency for the Scholte wave K_S is the highest frequency for which perfect cancellation can occur, and the interface wave amplitude is at its highest around this

frequency, resulting in very high reflection losses. Above it the substrate interaction is reduced and losses become negligible at significantly higher frequencies. A practical upper limit is about $2K_S$.

Combining both limits results in the overall condition $K_E < K < 2K_S$. In other words, ignoring the (small) imaginary part of c_2,

$$\cot\alpha_2 \ln\left(\frac{\zeta_0 - 1}{\zeta_0 + 1}\right) < 2K < \frac{2}{\left[(c_2/\sigma)^2 - 1\right]^{1/2}} \ln\left[\frac{(c_2/\sigma)^2 - 1}{\delta_2/(4\pi)}\right]. \tag{21}$$

3.3. Examples

To test inequality (9), six examples of layered seabeds with properties similar to that of Table 1 are selected from recent publications [3,20–22]. The relevant properties of these sediments are summarized in Table 2, showing the value of ζ_0 and, where applicable, the evanescent resonance frequency K_E. Also included for each seabed are the Scholte wave speed σ and critical frequency K_S. Notice that Tollefsen's Site I does not satisfy Eq. (9) and this explains the low losses observed for this case in his Fig. 1. (In principle, a Scholte wave can be generated for the Site I parameters, but only for an evanescent incident wave.) Interpretation for the Continental Shelf site from Hughes et al. [20], complicated by a non-zero shear speed in the sediment, is left for the discussion on sediment rigidity in Section 5. In all other cases, the criterion is satisfied and the predicted resonances are clearly visible in Hovem and Kristensen's [3] Fig. 3 at 48 Hz, Tollefsen's [21] Figs. 5a (12 Hz) and 6a (125 Hz) and Ainslie et al.'s [22] Fig. 4b at 15 Hz.

Two other sites from Ref. [20] ('Scotian Shelf' and 'Arctic Shelf') also have thin sediment layers but are not included in Table 2. The Scotian Shelf parameters are identical to those for the Continental Shelf except for the sediment thickness and water depth, so the only change would be a scaling of the frequencies f_E and f_S, which are inversely proportional to the sediment thickness.

Table 2
Summary of seabed properties from various sources, in order of increasing shear speed ratio c_3^s/c_1 from top to bottom

Source	c_2/c_1	c_3^p/c_1	c_3^s/c_1	ρ_3/ρ_2	ζ_0	c_2 (m/s)	K_E	h (m)	f_E (Hz)	σ (m/s)	δ_2 (Np/λ)	K_S	f_S (Hz)
TI	1.088	2.109	1.224	1.633	−0.421	1600	N/A	20.0	N/A	1345	0.055	3.53	44.9
HK	1.133	3.133	1.533	1.250	−1.352	1700	1.78	10.0	48.2	1560	0.092	3.74	101.3
TIII	1.172	2.655	1.552	1.378	−1.450	1700	1.38	3.0	124.9	1530	0.115	3.35	301.6
AB2	1.151	3.000	1.600	1.444	−1.761	1727	1.13	20.0	15.5	1613	0.058	4.51	61.9
Table 1	1.163	3.205	1.601	1.278	−1.694	1788	1.14	—	—	1653	0.100	3.71	—
HCS	1.219	3.767	1.644	1.182	−2.069	1780	0.76	1.75	122.4	1634	0.143	3.23	523.2
TII	1.088	3.605	2.091	1.576	−2.942	1600	0.82	18.0	11.7	1579	0.116	3.25	46.0

The frequency f is given by $(c_2/2\pi h)K$.
AB2 = Ainslie et al. [22] (B2).
HCS = Hughes et al. [20] (Continental Shelf).
HK = Hovem and Kristensen [3].
Table 1 = This paper (Table 1).
TI = Tollefsen [21] (Site I).
TII = Tollefsen [21] (Site II).
TIII = Tollefsen [21] (Site III).

The Arctic Shelf sediment has a very high shear speed (800 m/s) and cannot be treated, even approximately, as a fluid.

Ref. [22] results are actually for a layered sediment with sound speed ratio increasing from 1.091 at the top to 1.194 at the bottom. The c_2/c_1 value quoted here is an effective sound speed ratio required to reproduce approximately the same resonance frequency as the original profile [4].

Tollefsen's Sites I and II are marked in Fig. 4, representing the extremes (softest and hardest substrates) from Table 2. The other five cases are similar to each other and are represented in Fig. 4 by the Table 1 parameters.

3.4. Comparison with measured rock properties

The above examples, obtained from Refs. [20,21], are of acoustic measurements made at a number of sites where the conditions for generating interface waves are satisfied. We can now speculate on how likely it is for these conditions to arise more generally, by comparison with measured properties of real rocks. There are two questions of interest:

- Do commonly occurring rocks have shear speeds exceeding the derived threshold of 2.02 km/s?
- Are they covered by thin sediments?

Table 22 from Ref. [23] presents several hundred laboratory measurements of shear speed in rocks as a function of pressure in the range 10–1000 MPa (0.1–10 kbar). Excluding powdered rock, ash, tuff, breccia and all lunar material, only 10 out of about 300 tabulated values at 10 MPa (extrapolating from a higher pressure where necessary) are less than the threshold. These 10 are all for sedimentary rocks and soft basalts. Assefa and Sothcott [24] present shear speed measurements in their Table 1 for 18 samples of seafloor bedrock at low pressure (10 MPa), and of these only two values (both for basalts) are less than this threshold. A similar picture emerges from Table 7 of Ref. [23] (for rock from the oceanic crust and upper mantle), Fig. 16 of Ref. [5] (for basalts at 50 MPa) and also from Fig. 11 of Ref. [15] (for a variety of sedimentary, igneous and metamorphic rocks). Thus, the answer to the first question appears to be 'Yes' for many sedimentary rocks, most igneous rocks and all metamorphic rocks.

Regarding the second question, first one has to quantify what is meant by 'thin', and in this context we just mean, 'thickness of order one wavelength'. Assuming that a well-defined sediment layer exists at all, for any given sediment thickness, it is always possible to choose a frequency that meets this criterion. The answer to the second question, therefore, is 'Yes, but not necessarily for the frequencies of interest'.

This reasoning suggests that the conditions for the excitation of both varieties of interface wave are quite common, provided one is flexible about the choice of frequency. So why are their effects not observed more often? For a possible explanation, refer to the discussion of sediment rigidity in Section 5. There it is shown that even when the shear speed of the sediment layer is very low, its rigidity must be taken into account for a complete description. The effects due to the sediment shear waves then tend to obscure those of the interface waves.

4. Behaviour of reflection loss at resonance

The reflection loss vs. angle is now evaluated at the resonance frequency K_E for different values of ζ_0, with particular attention to behaviour close to $\zeta_0 = -1$. The value of ζ_0 is controlled by varying the sediment type [16] from very fine silt (grain diameter $\phi = 2^{-8}$–2^{-7} mm) to medium gravel ($\phi = 2^{+1}$–2^{+2} mm), keeping the substrate parameters fixed, for three different varieties of basalt. Correlations for continental terrace sediments are used to calculate geoacoustic properties from the grain size [6,7]. Fig. 5 shows reflection loss at resonance vs. angle θ_1 and sediment type for each of the three basalts which we categorize as 'hard' (density $\rho_3 = 3.0\,\mathrm{g/cm^3}$), 'medium' ($\rho_3 = 2.7\,\mathrm{g/cm^3}$) and 'soft' ($\rho_3 = 2.4\,\mathrm{g/cm^3}$). Compressional and shear speeds are calculated using the Christensen–Salisbury equations recommended by Hamilton [5,17]. The same recipe, described in Appendix A in more detail, was used to construct the parameters of Table 1 with a sediment porosity of 40% (fine sand) and basalt density $\rho_3 = 2.6\,\mathrm{g/cm^3}$.

For all the three substrate types, one can see a region of fine-grained sediments where losses are small for all angles, although for the hard basalt this region is confined to very fine silt only, with

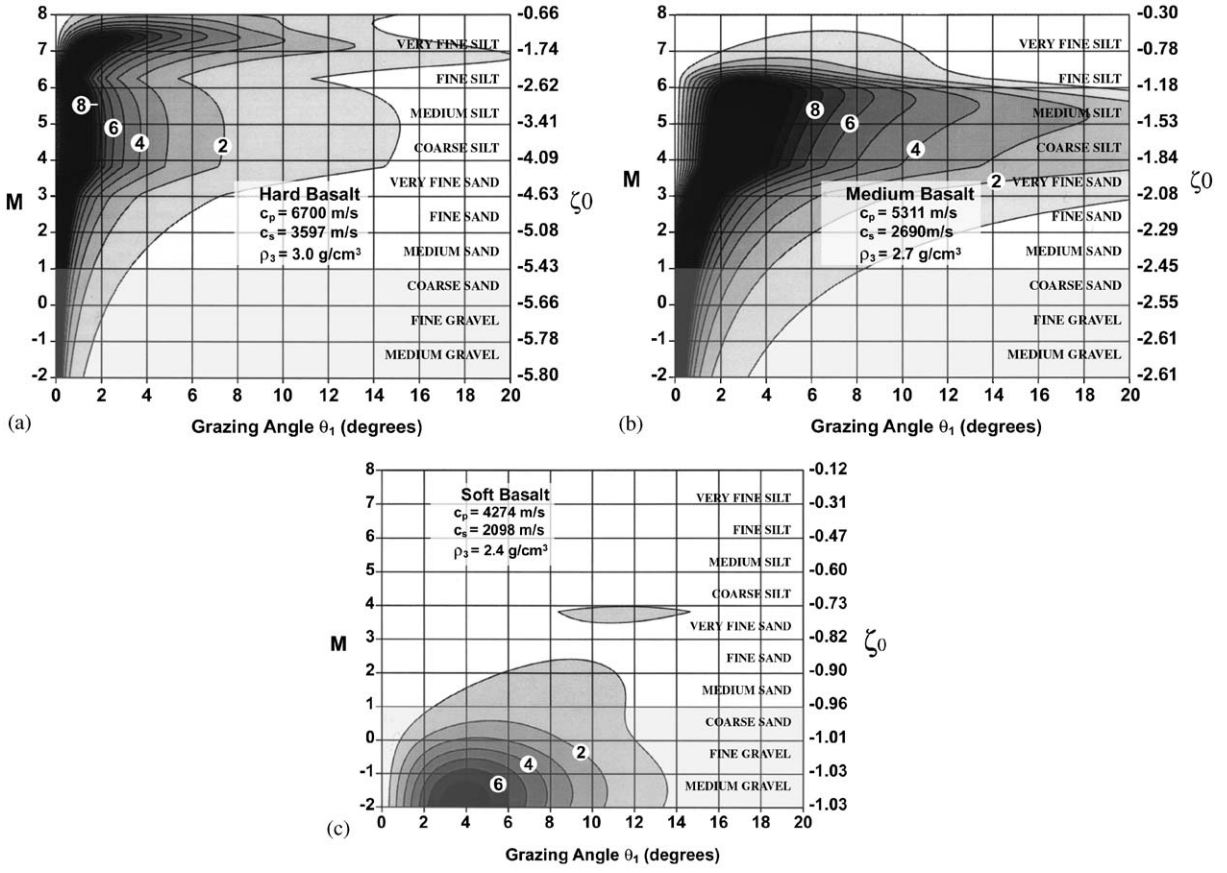

Fig. 5. Plane wave reflection loss at resonance vs. grazing angle θ_1 and sediment type for (a) hard basalt, (b) medium basalt and (c) soft basalt. Grain size M is given in phi units. Contour levels are in 1 dB steps starting at 1 dB.

$\phi \sim 2^{-8}$ mm. These low loss regions correspond to ζ_0 exceeding -1 so that inequality (9) is not satisfied. Strictly speaking, there is no resonance for such combinations, but for illustrative purposes Fig. 5 uses a nominal resonance frequency of

$$K_E = \left|\frac{\cot \alpha_2}{2}\right| \mathrm{Re}\left[\ln\left(\frac{\zeta_0 - 1}{\zeta_0 + 1}\right)\right] \tag{22}$$

for all values of ζ_0.

For medium basalt (Fig. 5b), there are three distinct regions: the low loss region ($\zeta_0 > -1$) for fine-grained sediments, a region exhibiting high loss near grazing incidence only, corresponding to coarse-grained sediments ($\zeta_0 < -2$), and an intermediate grade of sediments, corresponding roughly to ζ_0 values between –1 and –2, for which high losses extend over a broad range of angles. Notice that the Hamilton–Bachman equations have been extrapolated beyond their stated applicability, and this is indicated by the shaded regions of these graphs.

Fig. 5a for hard basalt is similar, except that the low loss region is almost non-existent. By contrast, the difference between Figs. 5b and c is striking, especially considering that the density of the soft basalt differs from that of medium basalt by just 11%. The difference is due to a reduction in the shear critical angle α_3^s to 43°, close to the critical value of 42° calculated in Section 3.1 above. This in turn means that $\zeta_0 + 1$ becomes a predominantly positive number and thus high losses are no longer possible for realistic fluid sediment properties. In fact, the resonance condition is only satisfied—in the extrapolated region of Fig. 5c—by very coarse-grained sediments (fine gravel and medium gravel). Predictions in this extrapolated region are unrealistic on three counts: firstly, the Hamilton–Bachman equations do not apply; secondly, even if they did, the material properties are such that the effects of sediment rigidity cannot reasonably be ignored; and finally, the extrapolated sediment densities in this region are greater than 2.4 g/cm^3, the density of the soft basalt substrate. For the finer grained sediments ($\phi < 2^{-2}$ mm), reflection losses are mostly less than 1 dB except for a small island of 1–2 dB for very fine sand of diameter $\phi \sim 2^{-4}$ mm. This island is due to a peak in the sediment attenuation coefficient estimated by Hamilton's correlation equation (see Appendix A). This same peak in attenuation is responsible for kinks (discontinuous gradients) in the contours of Figs. 5a and b at the same grain size.

What all the three basalt types have in common is that losses are highest when the value of ζ_0 is close to (and usually slightly less than) –1. Under these conditions, the value of ζ_{23} changes slowly with angle from ζ_0 at grazing incidence, to –1 at the Scholte angle. Therefore, a Scholte wave is excited, not just at the precise Scholte angle, but at a wide range of angles either side, merging into a single feature with the evanescent resonance at grazing incidence. The effects of the Scholte wave under these conditions are therefore broad not just in frequency but also in angle. Fig. 6 illustrates this point for the same three basalt substrates, with the sediment type chosen in each case to maximize the reflection loss at resonance. The y-axis is normalized by dividing by the evanescent resonance frequency. Figs. 6a and b both represent realistic combinations and the merged feature is clearly visible in both.

Long-range propagation in shallow water often relies on multiple reflections from the seabed at low angles. For the combinations considered in Fig. 6, within about an octave of the resonance frequency, most of the energy from the incident acoustic wave is converted into a Scholte wave at the sediment–substrate boundary. Thus, a dramatic effect on propagation loss can be expected in such cases.

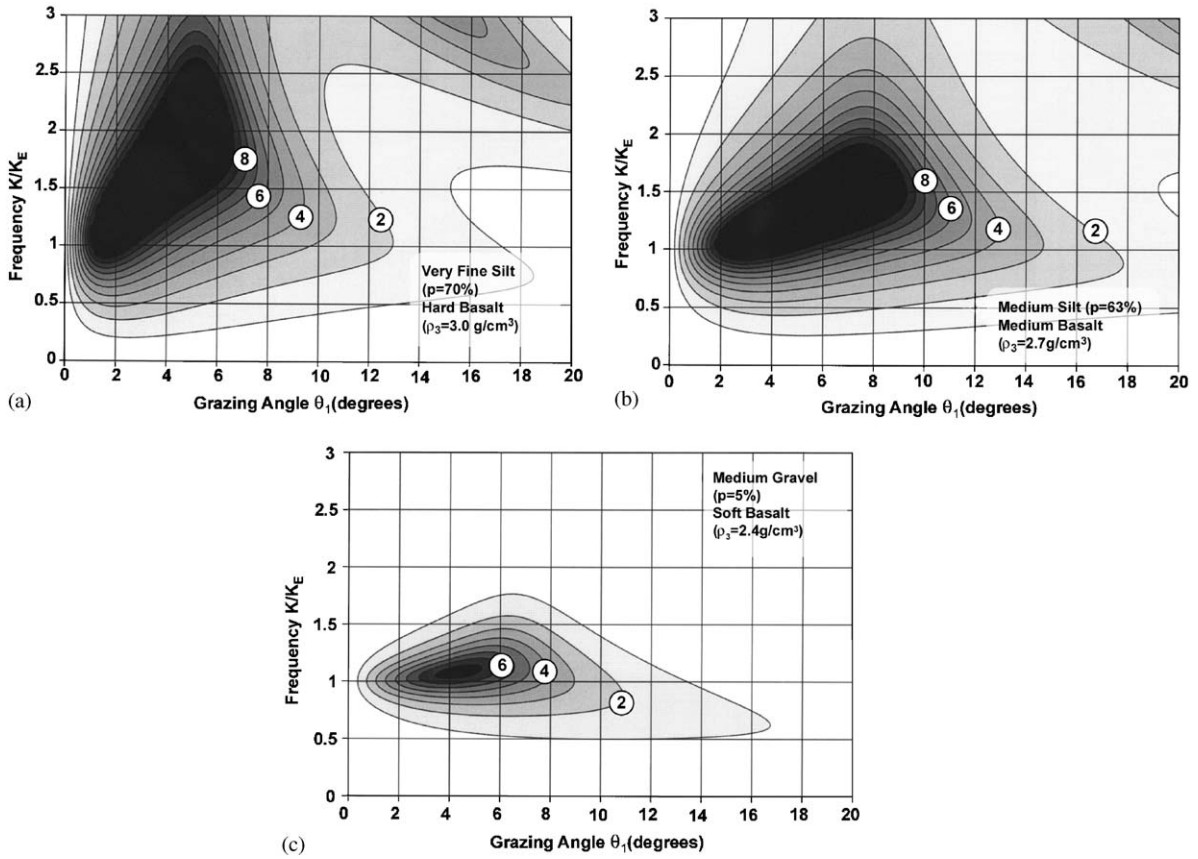

Fig. 6. Plane wave reflection loss vs. grazing angle θ_1 and normalized frequency K/K_E for (a) very fine silt sediment over a hard basalt substrate ($K_E = 5.82$), (b) medium silt over medium basalt ($K_E = 4.28$) and (c) medium gravel over soft basalt ($K_E = 1.67$). Contour levels are in 1 dB steps starting at 1 dB.

The third combination of medium gravel over soft basalt (Fig. 6c) is included for completeness, but is considered unrealistic for the reasons outlined above. The effect of sediment rigidity is discussed in Section 5 below.

5. Effect of sediment rigidity

So far, the effects of substrate rigidity (without which there can be no interface wave) have been modelled, but the possibility of shear waves in the *sediment* layer have been ignored by treating it as a fluid. This may seem reasonable on the grounds that the shear speed of silt or sand is small compared with its compressional speed, but in practice a small shear speed can have a disproportionately large effect on reflection loss and hence on shallow water propagation [20]. This is because at low frequency a train of shear waves is generated at the lower boundary and propagates up through the sediment layer [25]. These waves can influence the reflected field and have been identified with a series of resonances at regular intervals in frequency [20,26]. These are

referred to as quarter-wavelength ($\lambda/4$) resonances because they occur when the sediment thickness is equal to (odd) multiples of the shear wavelength divided by four. Interference between the resulting additional multipaths and the evanescent compressional wave results in a significant perturbation to Eq. (3) and hence also to Eq. (8). A convenient approximation to the reflection coefficient, valid for a small sediment shear speed, is provided by Eqs. (26) and (29) of Ref. [26], which we write in the form

$$r = \frac{\left[\left(1 + r_{23}^{ss}\right)\left(r_{12} + r_{23}^{pp}\right) - r_{23}^{ps} r_{23}^{sp}\right]}{\left[\left(1 + r_{23}^{ss}\right)\left(1 + r_{12} r_{23}^{pp}\right) - r_{12} r_{23}^{ps} r_{23}^{sp}\right]}, \tag{23}$$

where the $r_{23}^{\mu\nu}$ superscripts indicate the nature of the incident (μ) and reflected (ν) wave at the lower boundary. A detailed analysis of Eq. (23) is beyond the present scope, but its main properties are illustrated below by evaluating it for the Table 1 seabed parameters, except with a small non-zero sediment shear speed (c_2^s).

Fig. 7a shows the resulting reflection coefficient vs. frequency for a grazing angle of 2.5° and for shear speeds of 1, 10 and 100 m/s. The shear wave attenuation ($\beta_2^s = 2.19\,\mathrm{dB}/\lambda$) is chosen to match that of Refs. [20,26]. The fluid sediment case (not shown) follows the solid line ($c_2^s = 1\,\mathrm{m/s}$) apart

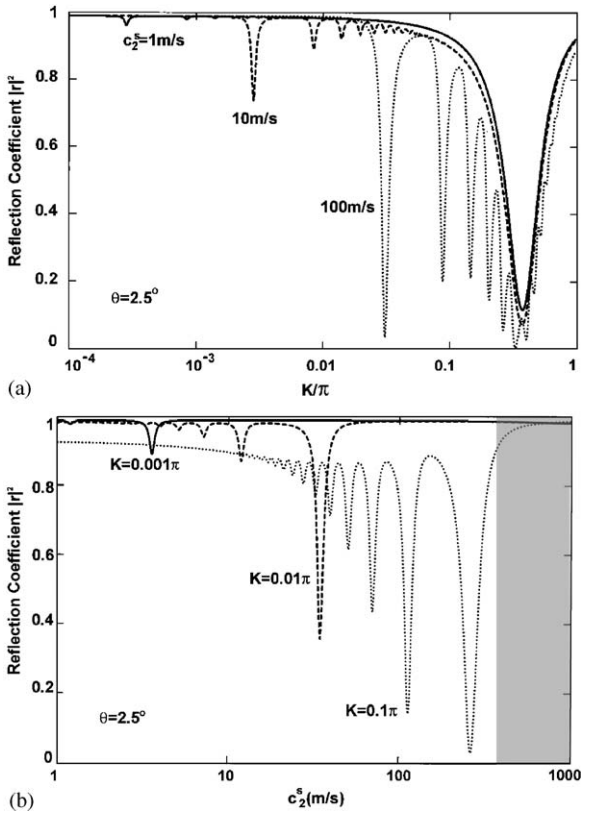

Fig. 7. Reflection coefficient $|r|^2$ vs. (a) frequency and (b) sediment shear speed. Other parameters are from Table 1 ($\theta_1 = 2.5°$).

from the weak resonances at very low frequency [$K/\pi = c_2^s/(2c_2^p) = 2.8 \times 10^{-4}$ and odd multiples]. As the shear speed is increased (to 10 m/s), the $\lambda/4$ resonances move to proportionately higher frequencies and become clearly visible. For the highest shear speed considered (100 m/s), the sequence of $\lambda/4$ resonances completely alters the character of the spectrum for values of K in the range 0.1–1.0.

Fig. 7b shows the variation of the low-frequency reflection coefficient, at three different frequencies, with increasing sediment shear speed. The shaded region on the right indicates a large shear speed for which the expansion leading to Eq. (23) is no longer valid. The expected sequence of $\lambda/4$ resonances is clearly visible. Notice in particular that significant losses (exceeding 3 dB per bounce) are predicted for shear speeds greater than about 30 m/s. For shear speeds exceeding 100 m/s the resonances depart noticeably from integer multiples of $\lambda/4$, as the shear wave propagation vector moves away from the vertical. In general, the resonance frequency K_n varies with both grazing angle θ_1 and sediment shear speed according to

$$K_n(\theta_1, c_2^s) = \frac{(2n-1)\pi c_2^s}{2c_2^p}\left[1 - \cos^2\theta_1 (c_2^s/c_1)^2\right]^{-1/2} \tag{24}$$

for integer $n > 0$. Rearranging for c_2^s gives the shear speed required for a resonance at a given frequency K_n

$$c_2^s(\theta_1, K_n) = \frac{2K_n c_2^p}{(2n-1)\pi}\left\{1 + \left[\frac{2K_n \cos\theta_1 c_2^p}{(2n-1)\pi c_1}\right]^2\right\}^{-1/2}. \tag{25}$$

Now return to the continental shelf parameters from Table 2, with a sediment shear speed of 170 m/s and attenuation 2.19 dB/λ. Because of the relatively large shear speed (> 100 m/s), one expects the evanescent resonance to be obscured by the shear wave effects, and this is confirmed by Fig. 8 showing $|r|^2$ vs. frequency for the Continental Shelf parameters at a grazing angle of 4°. A direct comparison is possible with the exact solution from Fig. 10 of Ref. [26], confirming the accuracy of Eq. (23) for this case. A similar masking effect can be seen in Tollefsen's [21] Figs. 5 and 6.

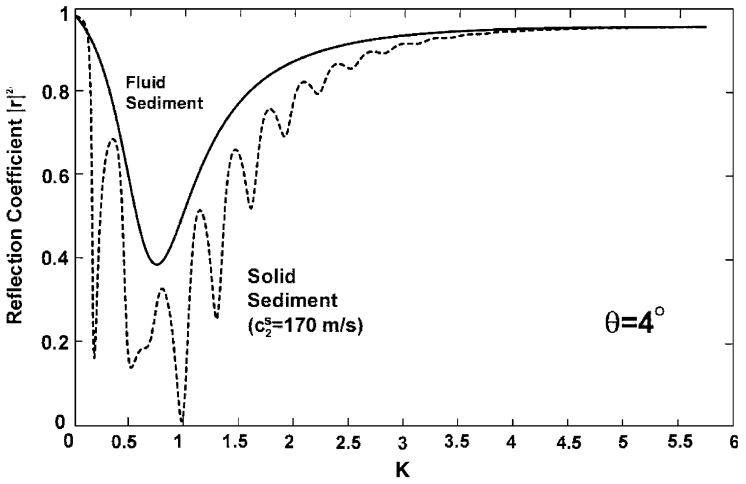

Fig 8. Reflection coefficient $|r|^2$ vs. frequency for HCS parameters from Table 2 ($\theta_1 = 4°$).

One can conclude that for sediment shear speeds exceeding 30 m/s, the sequence of shear wave resonances provides an important loss mechanism, comparable in magnitude with that for the evanescent resonance. Above 100 m/s, the shear wave mechanism begins to dominate. Sediment shear speeds exceeding 100 m/s are considered common [27], although Hamilton's regression formula has been shown to overestimate the shear speed of muddy sediments [28]. Significantly lower shear speeds, in the region of 30–80 m/s, have been observed in a variety of different near-surface coastal sediments [28–30]. While the effects of rigidity are important even for these lower speeds, the fluid sediment analysis provides an essential first step towards understanding the full problem. There is, nevertheless, a need for further work to extend the applicability of the Section 3 criteria to a solid sediment.

6. Summary and conclusions

The effect on seabed reflection loss of two types of interface waves is described, for the case of a thin fluid sediment layer overlying a solid substrate. One of these interface waves is the usual Scholte wave (sometimes referred to as a Stoneley wave). The other is an evanescent resonance excited near grazing incidence at a well-defined frequency. Particular attention is paid to the evanescent resonance that leads to high reflection loss. The key determining parameter is the sediment–substrate impedance ratio evaluated at grazing incidence, denoted by ζ_0, and high losses are shown to arise if the criterion $\zeta_0 < -1$ is met. This criterion cannot be satisfied unless the shear critical angle α_3^s of the solid exceeds an absolute minimum of 17.2° *regardless of sediment properties*. Taking into account the known correlations between geoacoustic properties of the seabed, it is unlikely to be satisfied unless α_3^s also exceeds about 42°. For a water sound speed of 1500 m/s, these critical angle thresholds translate to substrate shear speeds of 1570 and 2020 m/s, respectively. Both thresholds are shown to be exceeded for many commonly occurring bedrocks. The criterion is presented in both equation and graphical forms, as a lower limit on the compressional critical angles α_2 (Eq. (11) and Fig. 3) and α_3^p (Eq. (13) and Fig. 4). Illustrations are provided in the form of reflection loss vs. angle and frequency.

Particular combinations of sediment and substrate parameters, chosen such that the criterion $\zeta_0 < -1$ is only just met, give rise to an apparent broadening of the evanescent resonance in both angle and frequency. The reason for the broadening is actually a broadening of the Scholte wave in angle. When ζ_0 is close to (but slightly less than) –1, the conditions for exciting a Scholte wave are met across a wide range of angles near grazing incidence, and the two effects are thus no longer distinguishable as separate features in a plot of reflection loss vs. angle.

Complications due to the introduction of rigidity in the sediment layer result in a series of low-frequency resonances, which place an upper limit on the sediment shear speed for validity of the fluid sediment theory. For the cases considered, the excitation of sediment shear waves provides an important additional loss mechanism even for shear speeds as low as 30 m/s.

Acknowledgements

The author thanks Dr. A.J. Robins, Dr. S.G. Healy and Dr. D.G. Simons for their helpful comments, and Paul Anderson for the artwork.

Appendix A. Construction of seabed model

This appendix describes the procedure used to construct the geo-acoustic parameters for the seabed model used in the main text. All wave speeds are in units of m/s, densities in g/cm^3 and attenuations in dB/λ.

A.1. Substrate properties

The acoustic properties of bedrock vary with temperature and pressure [23,24]. For the present purpose, the equations due to Christensen and Salisbury [5] at 50 MPa are used as recommended by Hamilton [17]. For a given substrate density ρ_3, the compressional and shear speeds (for basalt) are calculated as:

$$c_3^p(\rho_3) = 2330 + 81\rho_3^{3.63}, \tag{A.1a}$$

$$c_3^s(\rho_3) = 1330 + 11\rho_3^{4.85}. \tag{A.1b}$$

These expressions are evaluated in Table 3 for $2\ \mathrm{g/cm^3} \leqslant \rho_3 \leqslant 3\ \mathrm{g/cm^3}$. The attenuation coefficients are $\beta_3^p = 0.1\ \mathrm{dB}/\lambda$ and $\beta_3^s = 0.2\ \mathrm{dB}/\lambda$ as recommended by Jensen et al. [31].

A.2. Sediment properties

The sediment sound speed and density are evaluated as a function of porosity p using the correlations published for continental terrace sediments by Hamilton and Bachman [6]

$$c_2(p) = 2502.0 - 23.45p + 0.14p^2, \tag{A.2}$$

$$\rho_2(p) = (157.6 - p)/57.8. \tag{A.3}$$

Similarly the attenuation coefficient is from Hamilton's [7] Fig. 5

$$\beta_2(p) = \frac{c_2(p)}{1000} \times \begin{cases} 0.2747 + 0.00527p, & p < 46.7\%, \\ 0.04903p - 1.7688, & 46.7 < p < 52\%, \\ 3.3232 - 0.0489p, & 52 < p < 65.5\%, \\ 0.7602 - 0.01487p + 0.000078p^2, & 65.5 < p < 90\%. \end{cases} \tag{A.4}$$

Notice the peak in attenuation at $p = 52\%$. This is the peak for very fine sand referred to in Section 4 of the main text. Notice also that $p = 65.5\%$ is used as the boundary between Hamilton's

Table 3
Basalt compressional and shear speeds vs. density, evaluated using Eq. (A.1)

ρ_3 (g/cm^3)	c_3^p (m/s)	c_3^s (m/s)
2.0	3333	1647
2.2	3747	1834
2.4	4274	2098
2.6	4929	2462
2.8	5731	2952
3.0	6700	3597

Table 4
Sediment properties vs. porosity p, evaluated using Eqs. (A.2)–(A.5)

p (%)	c_2/c_1	ρ_2/ρ_1	β_2 (dB/λ)	M	Sediment type
2.1	*1.596*	*2.63*	*0.70*	*−2*	
					Medium gravel
12.4	*1.452*	*2.45*	*0.76*	*−1*	
					Fine gravel
22.0	*1.335*	*2.29*	*0.80*	*0*	
					Coarse sand
30.9	*1.243*	*2.14*	*0.84*	+1	
					Medium sand
39.0	1.170	2.00	0.87	+2	
					Fine sand
46.4	1.115	1.88	0.89	+3	
					Very fine sand
53.1	1.074	1.76	1.20	+4	
					Coarse silt
59.1	1.044	1.66	0.70	+5	
					Medium silt
64.3	1.023	1.58	0.28	+6	
					Fine silt
68.8	1.009	1.50	0.17	+7	
					Very fine silt
72.6	1.000	1.44	0.14	+8	
					Coarse clay
75.6	0.994	1.38	0.13	+9	
					Medium clay
77.9	0.991	1.35	0.12	*+10*	

The italics indicate extrapolated parameters, some of which are unrealistic and included only for completeness.

[7] 'mixed sizes' and 'silt-clays' to avoid the small discontinuity that would otherwise arise through $p = 65.0\%$. The resulting sediment properties are shown in Table 4, at porosity values chosen to coincide with integer values of M according to Ref. [6]

$$p(M) = 22.01 + 9.24M - 0.365M^2 \quad (1 \leqslant M \leqslant 9), \tag{A.5}$$

where M is the grain size in phi-units [32] given by $M = -\log_2$ (mean grain diameter in mm). Although the validity of these equations is restricted to porosities in the range 35–85% (Eqs. (A.2) and (A.3)) and 36–90% (Eq. (A.4)), they are extrapolated to cases with $0 < p < 36\%$. Eq. (A.5) is also extrapolated for $M < 1$ and $M > 9$.

A.3. Water properties

The density of water is fixed at $\rho_1 = 1.025\,\mathrm{g/cm^3}$. The sound speed, $c_1 = 1537.9\,\mathrm{m/s}$, is determined from the sound speed ratio for Hamilton's [33] 'silty clay' ($p = 75.9\%$) of 0.994, from his Table IB.

References

[1] K.E. Hawker, Influence of Stoneley waves on plane-wave reflection coefficients: characteristics of bottom reflection loss, J. Acoust. Soc. Am. 64 (1978) 548–555.
[2] K.E. Hawker, The existence of Stoneley waves as a loss mechanism in plane wave reflection problems, J. Acoust. Soc. Am. 65 (1979) 682–686.
[3] J.M. Hovem, Å. Kristensen, Reflection loss at a bottom with a fluid sediment layer over a hard solid half-space, J. Acoust. Soc. Am. 92 (1992) 335–340.
[4] M.A. Ainslie, Interface waves in a thin sediment layer: review and conditions for high loss, Proc. Inst. Acoust. 21 (9) (1999) 33–47.
[5] N.I. Christensen, M.H. Salisbury, Structure and constitution of the lower oceanic crust, Rev. Geophys. Space Phys. 13 (1975) 57–86.
[6] E.L. Hamilton, R.T. Bachman, Sound velocity and related properties of marine sediments, J. Acoust. Soc. Am. 72 (1982) 1891–1904.
[7] E.L. Hamilton, Compressional-wave attenuation in marine sediments, Geophysics 37 (4) (1972) 620–645.
[8] J.M. Hovem, M.D. Richardson, R.D. Stoll (Eds.), Shear Waves in Marine Sediments, Kluwer, Dordrecht, 1991.
[9] L. Cagniard, Reflection and Refraction of Progressive Seismic Waves, Appendix II, McGraw-Hill, New York, 1962.
[10] C.L. Morfey, Dictionary of Acoustics, Academic Press, London, 2001.
[11] E. Strick, A.S. Ginzbarg, Stoneley-wave velocities for a fluid–solid interface, Bull. Seis. Soc. Am. 46 (1956) 281–292.
[12] D. Rauch, Experimental and theoretical studies of seismic interface waves in coastal waters, in: W.A. Kuperman, F.B. Jensen (Eds.), Bottom-Interacting Ocean Acoustics, Plenum, New York, 1980, pp. 307–327.
[13] M.A. Ainslie, Reflection and transmission coefficients for a layered fluid sediment overlying a uniform solid substrate, J. Acoust. Soc. Am. 99 (1996) 893–902.
[14] I. Tolstoy, C.S. Clay, Ocean Acoustics: Theory and Experiment in Underwater Sound, McGraw-Hill, New York, 1966.
[15] W.J. Ludwig, J.E. Nafe, C.L. Drake, Seismic Refraction, in: A.E. Maxwell (Ed.), The Sea, 4 Part 1, Wiley, New York, 1970, pp. 53–84.
[16] J.A. Udden, Mechanical composition of clastic sediments, Bull. Geol. Soc. Am. 25 (1914) 655–744.
[17] E.L. Hamilton, Sound velocity–density relations in sea-floor sediments and rocks, J. Acoust. Soc. Am. 63 (1978) 366–377.
[18] E.L. Hamilton, Vp/Vs and Poisson's ratios in marine sediments and rocks, J. Acoust. Soc. Am. 66 (1979) 1093–1101.
[19] G.H.F. Gardner, L.W. Gardner, A.R. Gregory, Formation velocity and density—the diagnostic basics for stratigraphic traps, Geophysics 39 (1974) 770–780.
[20] S.J. Hughes, D.D. Ellis, D.M.F. Chapman, P.R. Staal, Low-frequency acoustic propagation loss in shallow water over hard-rock seabeds covered by a thin layer of elastic-solid sediment, J. Acoust. Soc. Am. 88 (1990) 283–297.
[21] D. Tollefsen, Thin-sediment shear-induced effects on low-frequency broadband acoustic propagation in a shallow continental sea, J. Acoust. Soc. Am. 104 (1998) 2718–2726.
[22] M.A. Ainslie, A.J. Robins, M.K. Prior, Benchmark solutions of plane wave bottom reflection loss, J. Acoust. Soc. Am. 104 (1998) 3305–3312.
[23] N.I. Christensen, Seismic velocities, in: R.S. Carmichael (Ed.), Handbook of Physical Properties of Rocks, Vol. II, CRC Press, Boca Raton, FL, 1982 (Chapter 1).
[24] S. Assefa, J. Sothcott, Acoustic and petrophysical properties of seafloor bedrocks, SPE Formation Eval. 12 (1997) 157–163.
[25] P.J. Vidmar, Ray path analysis of sediment shear wave effects on bottom reflection loss, J. Acoust. Soc. Am. 68 (1980) 639–648.
[26] M.A. Ainslie, Plane-wave reflection and transmission coefficients for a three-layered elastic medium, J. Acoust. Soc. Am. 97 (1995) 954–961; erratum, J. Acoust. Soc. Am. 105 (1999) 2053.

[27] E.L. Hamilton, Acoustic properties of sediments, in: A. Lara Sáenz, C. Ranz Guerra, C. Carbó Fité (Eds.), Acoustics and ocean bottom, Consejo Superior de Investigaciones Científicas, Madrid, 1987, pp. 3–58.
[28] M.D. Richardson, E. Muzi, B. Miaschi, F. Turgutcan, Shear wave velocity gradients in near-surface marine sediment, in: J.M. Hovem, M.D. Richardson, R.D. Stoll (Eds.), Shear Waves in Marine Sediments, Kluwer, Dordrecht, 1991, pp. 295–304.
[29] S.E. Jones, C.F. Jago, Small-scale in situ measurements of S–H velocity in surficial sedimentary deposits: localised textural and biological controls, in: J.M. Hovem, M.D. Richardson, R.D. Stoll (Eds.), Shear Waves in Marine Sediments, Kluwer, Dordrecht, 1991, pp. 313–320.
[30] T.G. Muir, T. Akal, M.D. Richardson, R.D. Stoll, A. Caiti, J.M. Hovem, Comparison of techniques for shear wave velocity and attenuation measurements, in: J.M. Hovem, M.D. Richardson, R.D. Stoll (Eds.), Shear Waves in Marine Sediments, Kluwer, Dordrecht, 1991, pp. 283–294.
[31] F.B. Jensen, W.A. Kuperman, M.B. Porter, H. Schmidt, Computational Ocean Acoustics, 1994, American Institute of Physics, New York, p. 41.
[32] Anonymous, Coastal Sediment properties, Coastal Engineering Manual, Part III, Chapter 1, Department of the Army, New York, US Army Corps of Engineers, Washington, DC 20314–1000, available from http://www.usace.army.mil/inet/usace-docs/eng-circulars/ec1110-2-292/c-1.pdf.
[33] E.L. Hamilton, Geoacoustic modelling of the sea floor, J. Acoust. Soc. Am. 68 (1980) 1313–1340.